

Implications of XENON100 and LHC results for Dark Matter models (updated including 2012 data)

Marco Farina^a, Mario Kadastik^b, Duccio Pappadopulo^c,
Joosep Pata^d, Martti Raidal^b, Alessandro Strumia^{b,e}

(a) *Scuola Normale Superiore and INFN, Piazza dei Cavalieri 7, 56126 Pisa, Italia*

(b) *National Institute of Chemical Physics and Biophysics, Ravala 10, Tallinn, Estonia*

(c) *Institut de Théorie des Phénomènes Physiques, EPFL, CH-1015 Lausanne, Switzerland*

(d) *Department of Physics, University of Tartu, Estonia*

(e) *Dipartimento di Fisica dell'Università di Pisa and INFN, Italia*

Abstract

We perform a fit to the recent XENON100 data and study its implications for Dark Matter scenarios. We find that Inelastic Dark Matter is disfavoured as an explanation to the DAMA/LIBRA annual modulation signal. Concerning the scalar singlet DM model, we find that the XENON100 data disfavors its constrained limit. We study the CMSSM as well as the low scale phenomenological MSSM taking into account latest Tevatron and LHC data (1.1/fb) about sparticles and $B_s \rightarrow \mu\mu$. After the EPS 2011 conference, LHC excludes the “Higgs-resonance” region of DM freeze-out and XENON100 disfavors the “well-tempered” bino/higgsino, realized in the “focus-point” region of the CMSSM parameter space. The preferred region shifts to heavier sparticles, higher fine-tuning, higher $\tan\beta$ and the quality of the fit deteriorates.

1 Introduction

The best motivated candidates for the cold Dark Matter (DM) of the Universe [1] are Weakly Interacting Massive Particles (WIMPs) [2]. Indeed, a stable particle with a typical weak interaction cross section of 1 pb and a mass of order 100 GeV naturally produces the observed DM thermal relic abundance. Because the evidence for DM is purely gravitational, there are many particle physics models for WIMPs. Theoretically most appealing ones among those are the DM models based on supersymmetry (SUSY) [3] in which the DM is stable due to the existence of discrete Z_2 symmetry – the R-parity [4] or equivalently the matter parity [5]. Because the matter parity may occur also in the scalar extensions of the standard model (SM) [6], the scalar DM models are also well motivated from the underlying unified physics point of view.

The WIMPs have been searched for in the LEP, Tevatron and LHC experiments as well as in the underground DM direct detection experiments that detect DM recoils on nuclei. The history of DM direct detection experiments can be characterized with their sensitivity to the spin-independent DM-nucleon interaction cross section σ_{SI} as follows.

1. The non-relativistic DM annihilation cross section suggested by the observed cosmological DM abundance is $\sigma \sim 1/(T_0 M_{\text{Pl}}) \approx 3 \cdot 10^{-26} \text{ cm}^3/\text{s} = 10^{-36} \text{ cm}^2$. Such a large value of σ_{SI} is clearly excluded unless the DM particles have peculiar properties or their interactions are restricted to untested sectors.
2. DM that interacts with the Z boson: $\sigma_{\text{SI}} \approx \alpha^2 m_N^2 / M_Z^4 \approx 10^{-38} \text{ cm}^2$. Again, generic WIMPs of this type have been excluded.
3. DM that interacts with the Higgs boson: $\sigma_{\text{SI}} \approx \alpha^2 m_N^4 / M_{\text{DM}}^2 M_Z^4 \approx 10^{-43} \text{ cm}^2$, having assumed that the DM-DM-Higgs coupling is comparable with the weak coupling α .
4. DM that interacts with the W^\pm boson and consequently at loop level with nucleons [7], $\sigma_{\text{SI}} \approx \alpha^4 m_N^4 / (4\pi)^2 M_{\text{DM}}^2 M_W^6 \approx 10^{-46} \text{ cm}^2$, as predicted e.g. by Minimal Dark Matter [8].

Therefore, in the absence of new gauge bosons, the present most sensitive DM direct search experiments like CDMS [9], EDELWEISS [10] and XENON100 [11] are testing particle physics models in which DM is coupled to the Higgs boson or in which the DM interactions with matter occur only at loop level.

Although the CDMS, EDELWEISS and XENON100 searches for the DM have not given a discovery so far, there is a long-standing claim by DAMA/LIBRA [12] that sees an 8σ evidence for an annual modulation in the nuclear recoil signal of low-mass DM. Recently this claim received some support from the results of CoGeNT experiment [13]. In order to reconcile this result with the negative searches from other experiments, un-orthodox DM scenarios such as Inelastic Dark Matter (iDM) [14, 15] have been put forward. Testing all those scenarios is of utmost importance for understanding the nature of DM.

Recently the XENON100 experiment published new data after 101 days of data taking that probes values of the spin-independent DM/nucleus cross section down to $\sigma_{\text{SI}} \approx 7.0 \times 10^{-45} \text{ cm}^2$ [16]. They observed 3 signal candidate events with the expected background of (1.8 ± 0.6) events. This result leads to the most stringent limit on DM interactions today, and further constrains the best motivated DM models.

In this paper we perform a fit to the new XENON100 data and apply the results to constrain several model dependent as well as model independent scenarios of DM. First, motivated by the DAMA/LIBRA anomaly we study whether the iDM, as an explanation to the observed annual modulation, can survive the new XENON100 results. We find that this is not the case and the DAMA/LIBRA anomaly needs another explanation. After that we study the simplest possible DM model, the scalar singlet model.

However, most of our effort goes to the studies of SUSY models. We study the Constrained Minimal Supersymmetric Standard Model (CMSSM) as well as the low energy phenomenological MSSM (pMSSM). In doing that we apply also constraints on SUSY parameter space coming from the LHC at $\sqrt{s} = 7 \text{ TeV}$ with $1.1/\text{fb}$ of integrated luminosity, new data from D0, CMS and LHCb on $B_s \rightarrow \mu^+ \mu^-$, and new data from Tevatron on the top quark mass [17, 18, 19]. We find that the XENON100 data stringently constrains the “well-tempered” neutralino scenario [20], and excludes the corresponding “focus-point” parameter region of the CMSSM [21]. Therefore we perform a model independent analysis of that scenario. We derive constraints of

parameter	range	distribution
$v_0 \text{ km s}^{-1}$	200 - 240	Gaussian: 220 ± 10
$v_{\text{esc}} \text{ km s}^{-1}$	498 - 618	see [22]
\mathcal{L}_{eff}	$\pm 2\sigma$	see [16]

Table 1: *The parameters ranges for the XENON100 fits.*

new XENON100 data on the CMSSM and pMSSM parameter spaces and study the implications of those to the expected results in the LHC experiments. We find that, after EPS 2011 conference, the “Higgs-resonance” mechanism of DM freeze-out is completely excluded. The allowed CMSSM parameter space is pushed towards higher sparticle masses, the allowed range of $\tan\beta$ is constrained from below and from above, and the fine tuning of the parameters has become more severe. We show that the DM direct detection experiments and the LHC are complementary in constraining the supersymmetric parameter space.

The paper is organized as follows. In section 2 we perform the fit of new XENON100 data and apply this to iDM in section 3. In section 4 we study the scalar singlet model. In section 5 we study supersymmetric dark matter. We conclude in section 6.

2 Fit of XENON100 data

We perform a fit of the new data released by the XENON100 collaboration [16], taken between January and June 2010, which corresponds (before any cut) to an exposure of $101 \text{ days} \times 48 \text{ kg}$. XENON100 reports 3 events in the signal region which are consistent with an estimated background of 1.8 ± 0.6 events.

For fixed values of M_{DM} and σ_{SI} , the number of signal events expected in a given direct-detection experiment depends on astrophysical, nuclear and experimental parameters which are more or less well-measured. We build a global χ^2 including these extra parameters as nuisances and marginalize over them at the end.

On the astrophysical side one has to know both the local DM density, ρ_{\odot} , and the DM velocity distribution. In the standard halo model the latter is fixed to be a Maxwellian distribution with a given r.m.s. velocity v_0 , truncated at certain escape velocity v_E :

$$\frac{dN}{d\vec{v}} \equiv f(\vec{v}) \propto e^{-v^2/v_0^2} \theta(v - v_E). \quad (1)$$

The preferred values of the two velocities are $v_0 = 220 \text{ km s}^{-1}$ and $v_E = 544 \text{ km s}^{-1}$ [22]. We assume that v_0 has a Gaussian uncertainty of $\pm 10 \text{ km s}^{-1}$, and we allow for a 2σ variation of it in the fit. We take from [22] the probability distribution of the v_E parameter. The local DM density ρ_{\odot} is kept fixed to 0.3 GeV/cm^3 since the effect of its variation is just equivalent to an overall rescaling of σ_{SI} (the quantity really probed by direct detection experiments is their product $\sigma_{\text{SI}}\rho_{\odot}$).

In terms of this set of parameters the differential scattering rate per unit detector mass is

$$\frac{dR}{dE_{\text{nr}}} = N_T \frac{\rho_{\odot}}{M_{\text{DM}}} \int_{|\vec{v}| > v_{\text{min}}} d^3v \, v \, f(\vec{v}) \frac{d\sigma_{\text{DM} N}}{dE_{\text{nr}}}, \quad (2)$$

where N_T is the number of nuclei in the target per unit detector mass, M_{DM} is the DM mass and v_{min} is the minimal velocity which allows a nuclear recoil with energy E_{nr} . $\sigma_{\text{DM} N}$ is the nucleus-DM cross section.

We will be interested in spin-independent processes. Nuclear physics enters into the determination of form factors which modulates the cross section according to the momentum transfer:

$$\frac{d\sigma_{\text{DM } N}}{dE_{\text{nr}}} = \frac{m_N \sigma_{\text{SI}} (f_p Z + f_n (A - Z))^2}{2v^2 \mu_n^2 f_n^2} F^2(E_{\text{nr}}). \quad (3)$$

Here m_N is the nucleus mass, μ_n is the nucleon-DM reduced mass, and σ_{SI} is the spin-independent nucleon-DM cross section. We fix our choice of F to the standard Helm form factor [23]. We furthermore assume equal coupling strength to both protons and neutrons: $f_p \approx f_n = 1$.

The last important source of uncertainty comes from the experiment itself. In XENON100 the energy of a recoiling nucleus is inferred from the number of recorded photo-electrons (called *S1 signal*) emitted after the prompt relaxation of the excited nucleus. The relation between S1 and the recoil energy is given by

$$S1(E_{\text{nr}}) = 3.6 \text{ PE} \times E_{\text{nr}} \times \mathcal{L}_{\text{eff}}(E_{\text{nr}}). \quad (4)$$

The value of the function \mathcal{L}_{eff} at recoil energies (nuclear) smaller than 5 keV is not measured and must be extrapolated. Such extrapolation is crucial to put limits on light dark matter: the larger \mathcal{L}_{eff} is, the stronger the limits are. We use the recent \mathcal{L}_{eff} measurement from [16], based on [24], and we allow in our fit 2σ excursions from its central value.

In view of the small number of observed events we perform an event-by-event fit, such that we construct the χ -square [25]

$$\hat{\chi}_{\text{Xenon100}}^2(M_{\text{DM}}, \sigma_{\text{SI}}, \{p_i\}) = \hat{\chi}_{\{p_i\}}^2(M_{\text{DM}}, \sigma_{\text{SI}}) + \sum_i \chi_i^2(p_i), \quad (5)$$

where χ_i^2 is the one associated to the parameters themselves and $\hat{\chi}_{\{p_i\}}^2$ is the χ -square for fixed values of the parameters p_i (v_0 , v_{esc} and \mathcal{L}_{eff}), evaluated in terms of the S1 signal along the lines of [11]. We thus include both a Poissonian smearing of the signal and a Gaussian smearing of the energy measurement. The events are collected in the window $4 \text{ PE} \leq S1 \leq 30 \text{ PE}$. We use the acceptance from [16] and we model the background as a flat distribution in the signal region normalized to reproduce the expected number of background events.

We then marginalize $\hat{\chi}_{\text{Xenon100}}^2$ with respect to the nuisance parameters p_i defining

$$\chi_{\text{Xenon100}}^2(M_{\text{DM}}, \sigma_{\text{SI}}) = \min_{\{p_i\}} \hat{\chi}_{\text{Xenon100}}^2(M_{\text{DM}}, \sigma_{\text{SI}}, \{p_i\}), \quad (6)$$

where the minimum is taken in the range summarized in Table 1.

3 Inelastic Dark Matter

The DAMA collaboration reported an 8σ evidence for an annual modulation of their nuclear recoil signal [12] which is compatible with light dark matter scattering on nuclei. Such signal conflicts with other direct detection experiments and (as already remarked by the XENON100 Collaboration [16]) is strongly disfavored by XENON100 under the assumption of an elastic interaction of the dark matter with the Na nuclei of the DAMA detector. We show this in Fig. 1 where we plot the region favored by elastic scattering on sodium at DAMA together with the XENON100 exclusions. The DAMA confidence levels are obtained by a simple χ^2 fit of the first 12 bin of fig. 9 in [12], showing the energy dependence of the seasonal modulation.

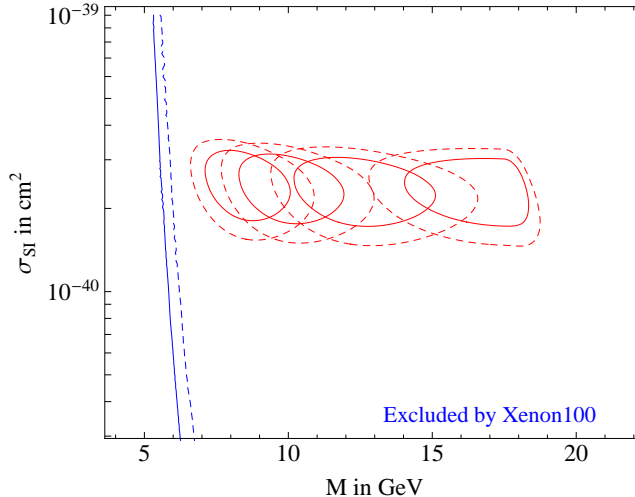


Figure 1: *The 95, 99.7% confidence level contours for 2 d.o.f. for the DAMA modulated signal under the assumption of elastic scattering on sodium atoms. We assume different values of the sodium quenching factor, 0.2, 0.3, 0.4 and 0.5, from right to left. The blue lines are the XENON100 exclusion curves at 95% (continuous curve), 99.7% (dashed) confidence level. We assume $v_0 = 220 \text{ km s}^{-1}$ and $v_{\text{esc}} = 544 \text{ km s}^{-1}$ for the DAMA fit. We neglect channeling.*

The strong bounds already from previous experiments, prompted theorists to consider Inelastic Dark Matter [14] (iDM), namely the idea that the DM detection process could be $\text{DM } N \rightarrow \text{DM}' N$ where the new state DM' is heavier than the DM state by an amount $\delta = M_{\text{DM}'} - M_{\text{DM}}$. It was pointed out that the modified kinematics could make the DAMA anomaly compatible with experiments, such as CDMS, that use lighter nuclei. Indeed the minimum DM velocity needed to scatter on a nucleus with mass m_N giving recoil energy E_{nr} is [14]

$$v_{\text{min}} > \sqrt{\frac{1}{2m_N E_{\text{nr}}}} \left(\frac{m_N E_{\text{nr}}}{\mu_N} + \delta \right), \quad (7)$$

where μ_N is the reduced mass of the DM/nucleus. For the mechanism to be effective the inelasticity mass splitting is assumed to be around 100 keV, which is the order of the typical nuclear recoil energy. By assuming progressively smaller tails of the uncertain DM velocity it is possible to avoid progressively stronger constraints from experiments with light nuclei. For the same reason it is possible to enhance the relative modulation in the signal claimed by DAMA.

Xenon nuclei have a mass very close to iodine which is, at DAMA, the dominant source of recoils for DM particles with mass above $\mathcal{O}(10 \text{ GeV})$. This fact, together with the high exposure of XENON100 allows to put strong constraints on the iDM hypothesis. This is shown in Fig. 2 where we plot 95% and 99.7% confidence level contours for the parameters favored by DAMA in the $(\delta, \sigma_{\text{SI}})$ plane, together with the XENON100 exclusion curves. The v_0 , v_{esc} and \mathcal{L}_{eff} parameters have been here fixed to their median values. We find that the iDM hypothesis to explain DAMA is disfavoured throughout its parameter space. This conclusion is sound, independent of the various uncertainties thanks to the similarity between Xe and I nuclei. This can be understood in a simple way [15]. The rate observed by DAMA can be written as

$$\mathcal{B} + \mathcal{S}(1 + a \cos \omega(t - t_0)), \quad (8)$$

where \mathcal{B} is a time-independent unknown background, \mathcal{S} is the mean DM signal and a describe the size of the modulation. $t_0 = 2 \text{ June}$, is where the peak of the modulation observed by DAMA

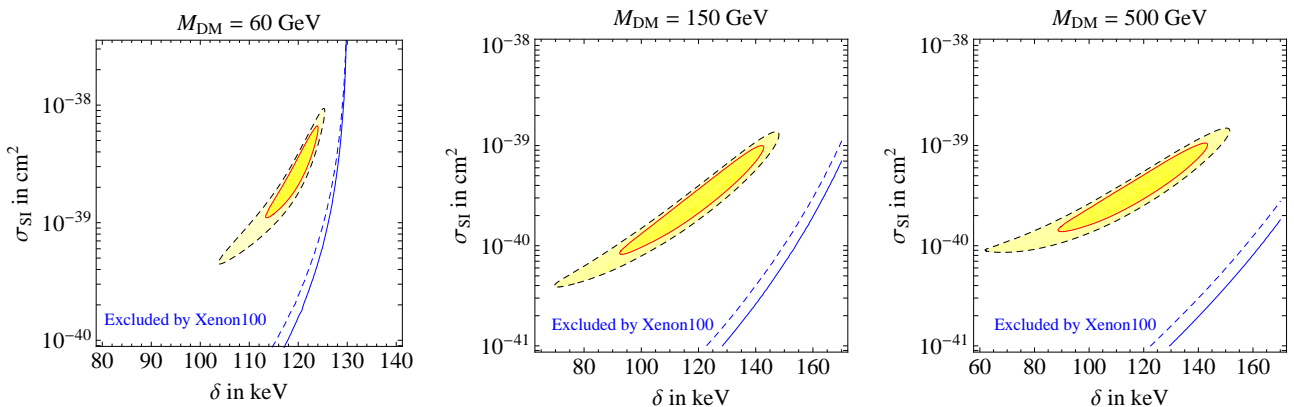


Figure 2: The 95, 99.7% confidence level contours for 2 d.o.f. for iDM fit to DAMA, together with the 95, 99.7% exclusion curves from XENON100 data (full and dashed respectively). We fix the iodine quenching factor to 0.085. Sodium quenching and channeling are irrelevant for these values of the mass.

is located. The size $a\mathcal{S}$ of the measured modulation is ~ 0.02 counts $\text{kg}^{-1} \text{day}^{-1}$ in the range $2 \text{ keV} \leq E_{\text{nr}} \leq 6 \text{ keV}$. Due to the iodine quenching factor, $q_I \approx 0.085$, this region translates to $23 \text{ keV} \leq E_{\text{nr}} \leq 70 \text{ keV}$ at Xenon. In the region of overlap between the former range and the acceptance window $8.4 - 44.6 \text{ keV}$, the DM scattering rate at Xenon is given by

$$R_{\text{Xenon100}} \sim A \times \epsilon \times \mathcal{S} (1/a + \cos \omega(t - t_0)). \quad (9)$$

ϵ and A are respectively the efficiency of the XENON100 cuts and its acceptance. Together they amounts to roughly 0.2. Integrating eq. (9) over the energy range and over the time of Xenon data-taking one finds

$$N_{\text{Xenon100}} > \mathcal{O}(50) \text{ events}, \quad (10)$$

where we folded in the exposure and we used $a < 1$. It is thus clear where the exclusion curves shown in Fig. 2 comes from.

4 Scalar singlet Dark Matter model

We consider a DM model obtained adding to the Standard Model a Dark Matter real singlet scalar field S coupled to the Higgs doublet H as described by the following Lagrangian [26, 27, 28, 29]:

$$\mathcal{L} = \mathcal{L}_{\text{SM}} + \frac{(\partial_\mu S)^2}{2} - \frac{m^2}{2} S^2 - \lambda S^2 |H|^2, \quad (11)$$

invariant under the matter parity $S \rightarrow -S$, the discrete gauge symmetry of scalars carrying $B - L$ [6]. S is the DM field and its mass is given by $M_{\text{DM}}^2 = m^2 + \lambda V^2$ with $V = 246 \text{ GeV}$. So the model has 2 free parameters, M_{DM} and λ . Assuming that the relic DM abundance equals its cosmologically measured value the model is able of predicting the relation in the plane $(M_{\text{DM}}, \sigma_{\text{SI}})$ plotted in Fig. 3. Given that the Higgs boson mass is also presently unknown, we plotted such relation for a few values of the Higgs mass: 115 GeV (green, favored by precision

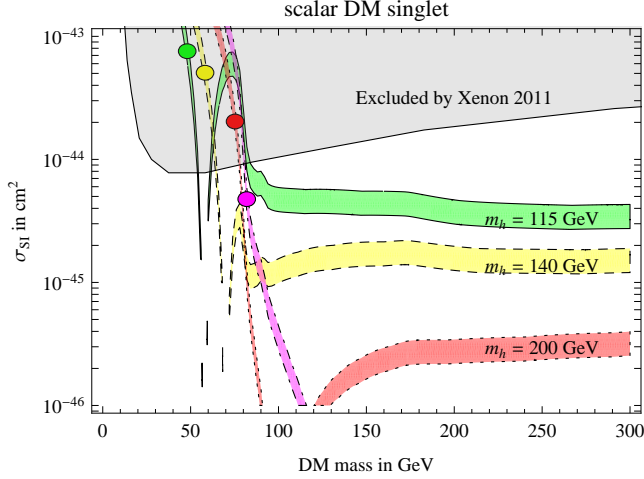


Figure 3: Predictions of the scalar singlet model for a few values of the Higgs boson mass: 115 GeV (green), 140 GeV (yellow), 200 GeV (red), 300 GeV (magenta). The dots are the predictions of the constrained model of [6, 30].

data), 140 GeV (yellow, compatible with precision data), 200 GeV (red, disfavored by precision data); 300 GeV (magenta, strongly disfavored by precision data).

The very small σ_{SI} predicted around $M_{\text{DM}} = m_h/2$ is due to the Higgs resonance enhancement of the cosmological DM annihilation rate. This quantity is computed as in [30], already including the 3 body final states whose relevance was emphasized in [31].

In absence of a theoretical motivation for having m comparable to the Higgs mass, [6, 30] considered the case $m = 0$, such that the model has one parameter less and is able of predicting a point in the plane $(M_{\text{DM}}, \sigma_{\text{SI}})$. Such prediction is also shown in Fig. 3, for the same values of the Higgs boson mass.

We remark two uncertainties not explicit from the plot. First, the XENON100 exclusion bound is plotted assuming $\rho_\odot = 0.3 \text{ GeV}/\text{cm}^3$ for the local DM density. This is the canonical value routinely adopted in the literature, with a typical associated error bar of $\pm 0.1 \text{ GeV}/\text{cm}^3$. Recent computations found a higher central value closer to $0.4 \text{ GeV}/\text{cm}^3$ [32] that would imply stronger bounds on the cross section σ_{SI} .

Second, the prediction for the conventional spin-independent DM/nucleon cross section is:

$$\sigma_{\text{SI}} = \frac{\lambda^2 m_N^4 f^2}{\pi M_{\text{DM}}^2 m_h^4}, \quad (12)$$

where f parameterizes the nucleon matrix element:

$$\langle N | m_q \bar{q}q | N \rangle \equiv f_q m_N [\bar{N}N], \quad f = \sum_{q=\{u,d,s,c,b,t\}} f_q = \frac{2}{9} + \frac{5}{9} \sum_{q=\{u,d,s\}} f_q. \quad (13)$$

The main uncertainty comes from f_s . The recent analyses use $f = 0.56 \pm 0.11$ [33], or $f = 0.30 \pm 0.015$ [34], in agreement with the lattice results [35] and phenomenological determination [36]. Here and in the following we assume the default value in the MICROMEGAS code: $f = 0.467$ [37].

quantity	experiment	Standard Model
$\alpha_3(M_Z)$ [46]	0.1184 ± 0.0007	parameter
m_t [47]	173.1 ± 0.9	parameter
m_b [48]	4.19 ± 0.12	parameter
$\Omega_{\text{DM}} h^2$ [49]	0.112 ± 0.0056	0
δa_μ [50]	$(2.8 \pm 0.8) 10^{-9}$	0
$\text{BR}(B_d \rightarrow X_s \gamma)$ [51]	$(3.50 \pm 0.17) 10^{-4}$	$(3.15 \pm 0.23) 10^{-4}$
$\text{BR}(B_s \rightarrow \mu^+ \mu^-)$ [19]	$(0.9 \pm 0.6) 10^{-8}$	$(0.33 \pm 0.03) 10^{-8}$
$\text{BR}(B_u \rightarrow \tau \bar{\nu})/\text{SM}$ [52]	1.25 ± 0.40	1

Table 2: *The data we fit, together with LHC and XENON100 bounds.*

5 Supersymmetry

In this section we study the impact of new XENON100 data on constraining SUSY models. We first consider the CMSSM, the most popular SUSY model with an unified scalar mass m_0 , an unified gaugino mass $M_{1/2}$ and an unified trilinear scalar A -term at the GUT scale. Given that XENON100 adds to many other experimental constraints, we perform a global fit to all relevant data as described in the next subsection. Most importantly, we include the recent CMS and ATLAS constraints on the CMSSM parameters space that are based on the LHC data with 1.1/fb presented in july 2011. Our fits extend the previous ones obtained in the similar studies in [38, 39, 40, 41, 42, 44, 45] without EPS 2011 data.

One of the results of our research is that the “well-tempered” neutralino scenario is stringently constrained by the XENON100 new result. Motivated by that we perform a generic analyses of the “well-tempered” neutralino and show that, quite model independently, this scenario is now stringently constrained.

Finally we relax the CMSSM constraints on the particle spectrum coming from the unification relations and study a generic low energy phenomenological MSSM, the pMSSM. We identify the generic XENON100 constraints on pMSSM.

5.1 Global fit of supersymmetric models

Global fits of the SUSY models have recently been performed by several groups in the context of LHC studies, and our results agree with them. Therefore we focus on the impact of the new XENON100 data in constraining SUSY models. Here, we briefly describe our procedure, and the differences with respect to previous approaches.

We perform a random scan of the parameter space and calculate the sparticle spectrum as well as DM relic abundance using the MICROMEGAS public code [37]. We vary the relevant input SM parameters (m_t , α_3 , m_b) within 5σ experimental errors assuming a Gaussian distribution. The CMSSM parameters (m_0 , $M_{1/2}$, A_0 , $\tan\beta$, $\text{sign}(\mu)$) are generated randomly in the ranges $(m_0, M_{1/2}) \sim (0, 4000)$ GeV, $A_0 \sim (-3m_0, 3m_0)$, $\tan\beta \sim (1, 60)$ and $\text{sign}(\mu) = \pm 1$ with a flat distribution. Using MICROMEGAS we compute all observables for each sampling point and select those rare cases that reproduce all experimental data within 5σ errors.

We do not use any special technique such as Markov chains, which makes the scanning more efficient, but that might lead to missing some local best-fit regions. Using the computing power of the Baltic Grid we get about 200,000 good points that satisfy all the experimental criteria.

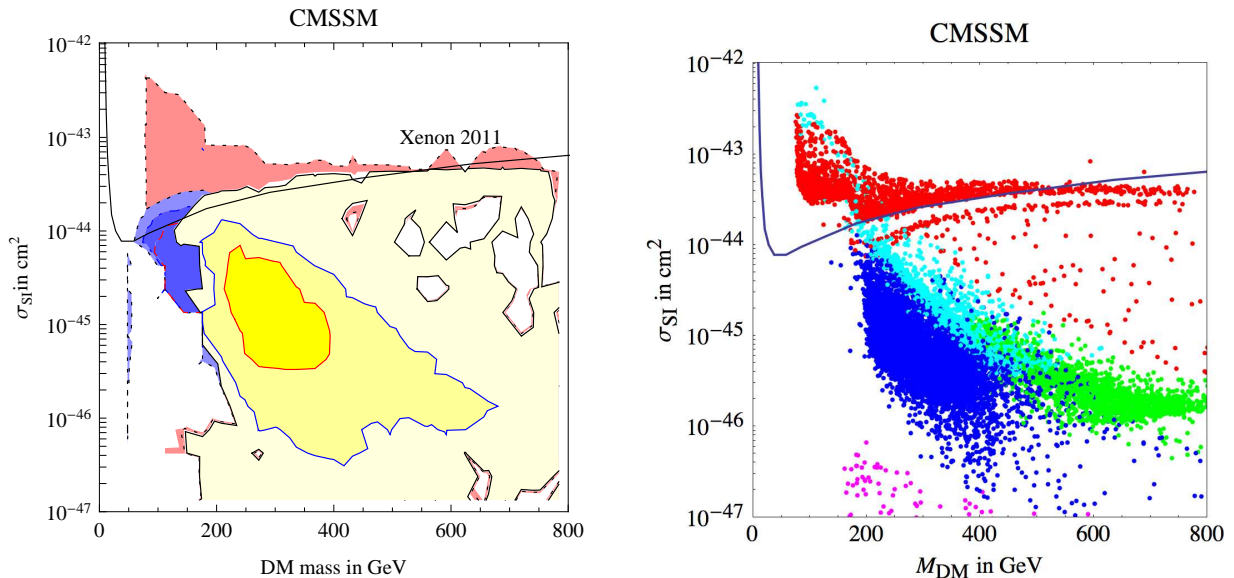


Figure 4: *The $(M_{\text{DM}}, \sigma_{\text{SI}})$ plane in the CMSSM. In the left panel we show the global fit: the yellow regions surrounded by continuous contours are the best fit including the XENON100 and LHC data, at 68, 95, 99.7% confidence levels for 2 d.o.f. The red (blue) regions surrounded by dashed contours are the corresponding regions now excluded by XENON100 (LHC). In the right panel we show points with $\Delta\chi^2 < 4^2$, colored according to the DM annihilation mechanism. The red dots in the upper region excluded by the XENON100 correspond to the “well-tempered” neutralino, green via the heavy Higgs resonance, cyan via neutral Higgses with $\tan\beta$ -enhanced couplings, blue via slepton co-annihilations, magenta via stop co-annihilations.*

For such points we compute the global χ^2 using the data summarized in Table 2:

$$\chi^2 = \chi_{\text{SM parameters}}^2 + \chi_{\text{observables}}^2 + \chi_{\text{LHC}}^2 + \chi_{\text{Xenon100}}^2. \quad (14)$$

Notice that we do not include electroweak precision observables, that do not have a significant impact on the result, and that are not well approximated simply by the oblique parameters [53].

In this work we perform a purely phenomenological fit, considering values of the sparticles masses significantly above the weak scale (up to 4 TeV), ignoring the theoretical issue of naturalness (see [54, 55] for a recent analysis). Technically, this is achieved as follows: when plotting the χ^2 as function of one or two parameters, we minimize it with respect to all other parameters. The fit is mainly driven by the DM abundance and by the apparent anomaly in the anomalous magnetic moment of the muon, and agrees with the fits in [40, 41, 56]. Given that it might not be a real anomaly, we also show regions at relatively high confidence levels.

We keep the nuclear matrix elements and the DM local density fixed to their default values in MICROMEGAS, as already discussed in the previous section.

5.2 The CMSSM results

Fig. 4a shows our global CMSSM fit for the DM mass M_{DM} and spin-independent DM-nucleus cross section σ_{SI} measured by XENON100 experiment. The yellow regions surrounded by continuous contours are the best fit regions including the XENON100 and LHC data, at 1, 2 and

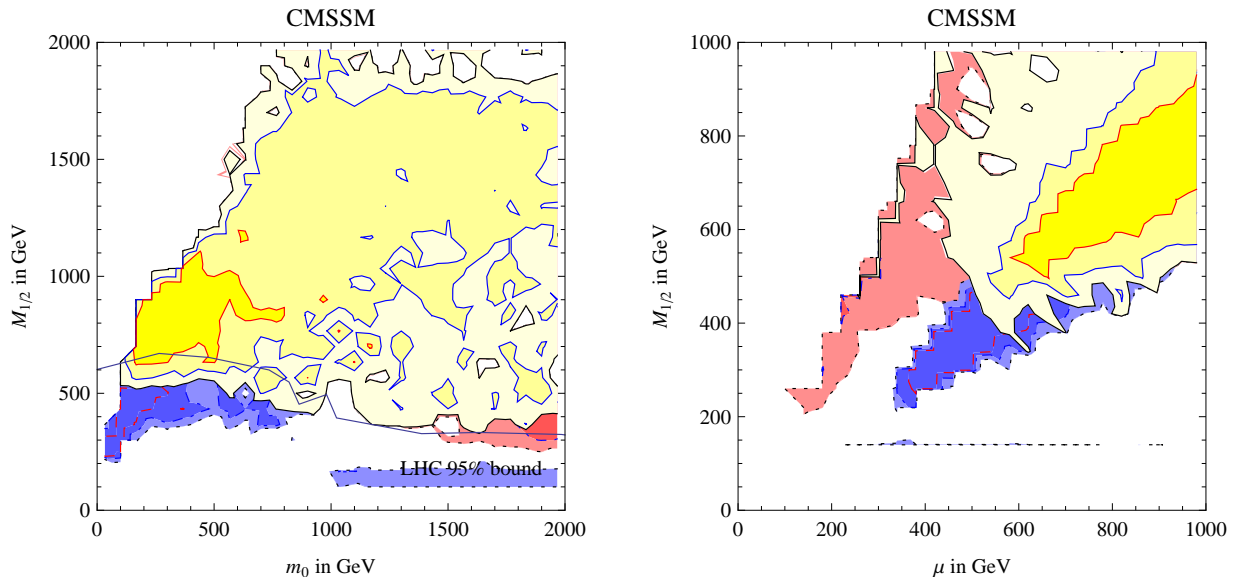


Figure 5: *Global CMSSM fits in $(m_0, M_{1/2})$ (left) and in $(\mu, M_{1/2})$ (right) planes. The red (blue) contours are excluded by XENON100 (LHC), other details are as in Fig. 4a.*

3σ level (68, 95, 99.7% confidence levels for 2 d.o.f.). We also show, as red regions surrounded by dashed contours, the previous best-fit regions at the same confidence levels now excluded by XENON100 at more than 3σ . Obviously, such excluded regions lie around the XENON100 exclusion bound at 90% confidence level (the continuous curve in the figure).

Within the CMSSM, thermal freeze-out of neutralino DM can reproduce the observed DM cosmological abundance according to a few qualitatively distinct mechanisms, that correspond to different fine-tunings. To interpret this result we therefore discriminate such distinct cases, plotting in Fig. 4b the points of the CMSSM parameter space (also imposing a reasonably good global fit, $\Delta\chi^2 < 4^2$) colored according to their dominant DM annihilation mechanisms. We identify the following distinctive regions:

1. Red points (“arm” in the upper part of the plot) have $|\mu| \approx M_1$ such that the lightest neutralino has a significant Higgsino component (“well-tempered” neutralino [20]). In the CMSSM this happens in the fine-tuned region with large m_0 and small μ in the so-called “focus-point” region [21]. The double structure of the “arm” in Fig. 4b shows that both signs of the μ parameter can give the correct DM relic abundance while $\mu > 0$ is favored by the $(g - 2)_\mu$ anomaly. Comparison with Fig. 4a shows that the new XENON100 data excludes or disfavors this scenario.
2. Blue points (around the center of the plot) have $m_{\tilde{\ell}} \approx M_{\text{DM}}$, corresponding to slepton co-annihilations. They provide the best global fit.
3. Green points (around the bottom-right part of the figure) have $M_{\text{DM}} \approx m_A/2$, corresponding to the resonant DM annihilations mediated by the heavy CP-odd Higgs boson A . The light-Higgs resonance (that arises for $M_{\text{DM}} \approx m_h/2$ and consequently implies a relatively light gluino) has now been excluded by the new bounds on the gluino mass obtained by the CMS and ATLAS collaborations after 1.1/fb of data.

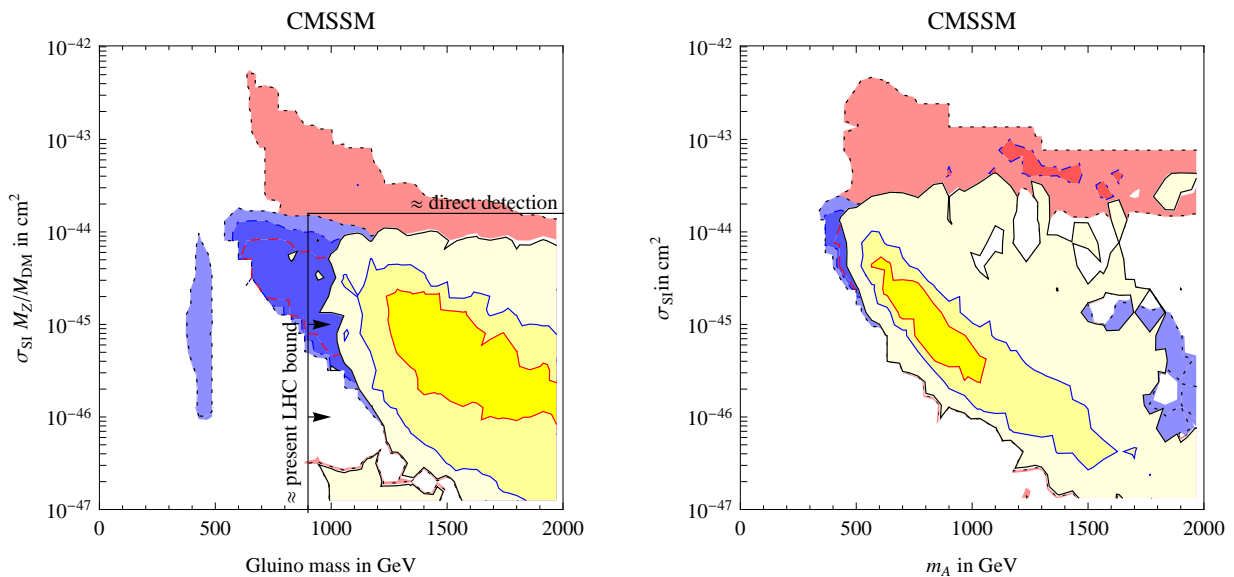


Figure 6: Global CMSSM fits in $(M_{\tilde{g}}, \sigma_{\text{SI}})$ (left) and in $(m_A, \sigma_{\text{SI}})$ (right) planes. The red (blue) contours are excluded by XENON100 (LHC), other details are as in Fig. 4a.

4. Cyan points represent parameters in which one moves away from Higgs resonances (we arbitrarily assume a 10% off-degeneracy to discriminate from the previous case) but the DM annihilation processes are still mediated via all neutral Higgses in s -channel. A large enough Higgs couplings to the SM fermions and to DM is obtained thanks to $\tan \beta > 45$ and to a non-negligible Higgsino component of the DM neutralino. Consequently some of these points have a large direct detection cross section.
5. Magenta points (at very low σ_{SI}) correspond to stop co-annihilations. The latter region is/will be further constrained by the LHC data that presently excludes light stops.

We remark that, within the CMSSM, the LEP and LHC bounds have excluded one more mechanism that was considered more plausible because its non-fine-tuned nature: the bino annihilations via light slepton exchange in t -channel. In the light of our results the experimental data favours slepton co-annihilation as the mechanism for generating neutralino thermal relic abundance. This result is a consequence of the fact that the fit is largely dominated by the measurement of muon anomalous magnetic moment that requires relatively light sleptons.

In the light of these considerations, we can now discuss the global CMSSM fits for other parameters. Fig. 5 shows some 2-dimensional fits as indicated in the figure. We see that XENON100 strongly disfavors regions with small $|\mu|$ and partly also with small $M_{1/2}$ (the very small allowed region at 3σ level for small $M_{1/2}$ below the red excluded region corresponds to the Higgs resonance DM annihilation mechanism). Within the CMSSM a small $|\mu|$ can be realized in the “focus-point” scenario that requires a multi-TeV m_0 . Such a region was previously not favored by global fits and is now further disfavored by the XENON100 bound that disfavors a neutralino DM with a significant higgsino component. The fact that small values of $|\mu|$ below 400 GeV are now excluded by XENON100 data is perhaps one of the most important results of our work.

Fig. 6a compares the LHC prospects (here characterized by the approximate gluino mass reach), with the prospects of direct detection experiments (characterized by $\sigma_{\text{SI}} M_{\text{DM}}/M_Z$, which

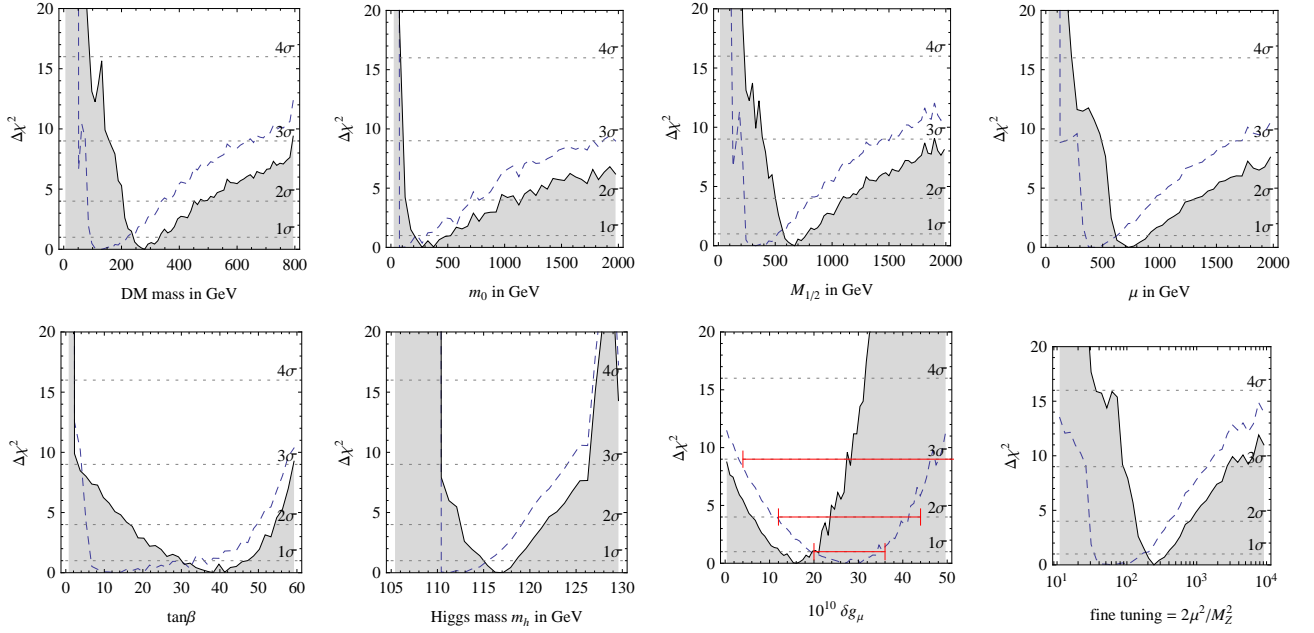


Figure 7: Global CMSSM fit before (dashed curve) and after (continuous curve) the XENON100 and LHC results. In the upper panels we fit the DM mass (left) the m_0 (middle left), $M_{1/2}$ (middle right), μ (right) parameters; in the lower panels we fit $\tan\beta$ (left), the Higgs mass m_h in GeV (middle left), the muon $g-2$ (middle right) and the fine-tuning parameter (right).

is the only parameter probed by experiments when M_{DM} is much heavier than the target nucleus). We see that LHC excluded the Higgs resonance region, that within the CMSSM necessarily has a light gluino with mass $M_3 \approx 400$ GeV, and reached the best-fit region. On the other hand, Fig. 6b shows that, after XENON100, there is a clear correlation between the spin-independent DM direct detection cross section and m_A . Although the XENON100 results exclude only a very small region of the parameter space at low values of m_A , this implies that the CMSSM charged Higgs boson mass must exceed $M_{H^\pm} > 400$ GeV and is inaccessible at the 7 TeV LHC.

Finally, Fig. 7 shows our fits for the DM mass and for a few key parameters: m_0 , $M_{1/2}$, $\tan\beta$, m_h and $2\mu^2/M_Z^2$ (which is a simple measure of fine-tuning, closely related to the μ term). In all cases new data had a significant impact: the exclusion of lighter sparticles, moves the best fit to higher sparticle masses and consequently to higher $\tan\beta$ in order to fit the $g-2$ anomaly. As shown in the $g-2$ panel, there starts to be some tension between its experimental measurement (error bands) and the CMSSM predictions. Adding the LHC and Xenon100 bounds, the global χ^2 at the best-fit point worsens by $\Delta\chi^2 \approx 4.3$. Furthermore, the lower right panel shows that the fine-tuning grows up to the few hundred range (for a dedicated discussion see the updated version of [54]).

5.3 “Well-tempered” neutralino

As we have shown, within the CMSSM, the XENON100 result has interesting implications on the “well-tempered” neutralino [20]. Here we study this scenario of DM generation in SUSY models in a model-independent way. Within the MSSM, the neutralino is a mixed state of

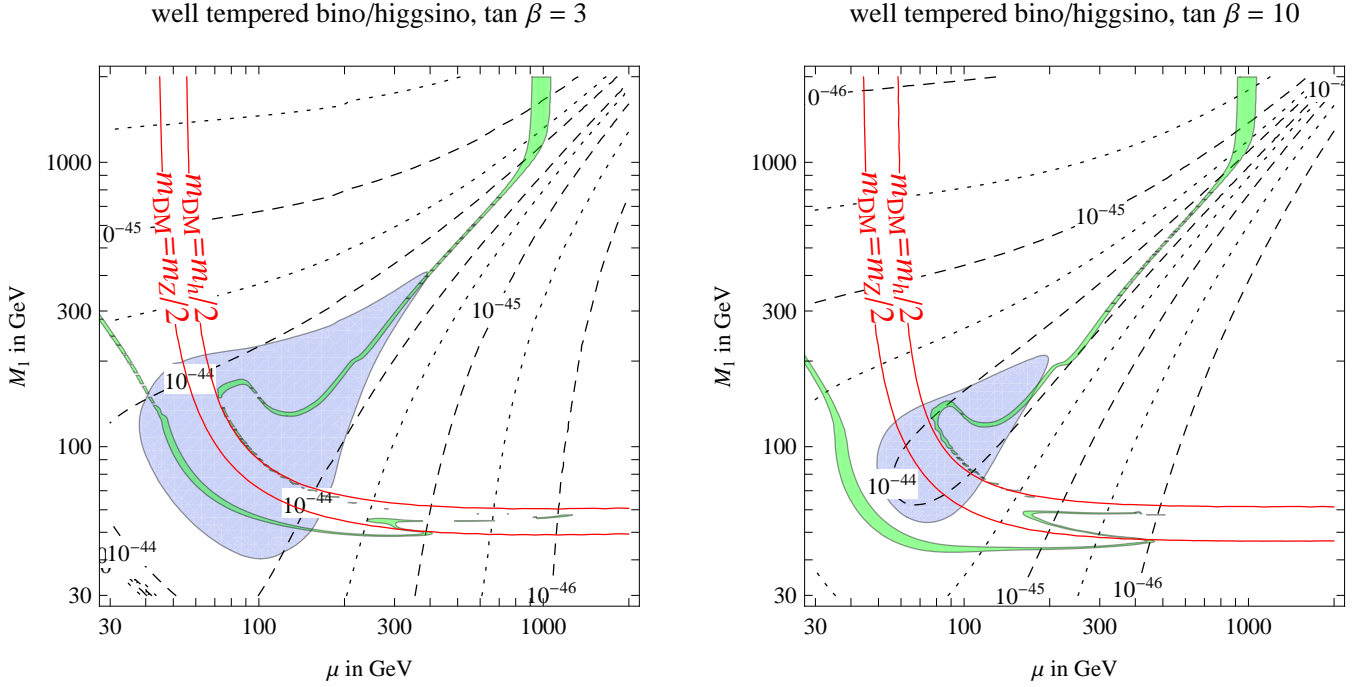


Figure 8: *Model independent “well-tempered” neutralino scenario. The 3σ range for the cosmological DM abundance is reproduced within the green strip. The gray region is excluded by XENON100 [16].*

bino, wino, higgsino. None of them, in a pure state, allows thermal DM with a weak scale mass $M_{\text{DM}} \approx M_Z$:

- The pure higgsino couples to the Z too strongly, such that for $M_{\text{DM}} \approx M_Z$ its thermal abundance is too low (the cosmological abundance is obtained for a heavy $M_{\text{DM}} \approx 1$ TeV higgsino); furthermore, for the same reason it is experimentally excluded by direct searches.
- The pure wino similarly has too much co-annihilations with charged winos, such that for $M_{\text{DM}} \approx M_Z$ its thermal abundance is too low (the cosmological abundance is obtained for a heavier $M_{\text{DM}} \approx 2.7$ TeV taking into account electroweak Sommerfeld effects [57]). Contrary to the previous case, having no coupling to the Z it is allowed by direct searches.
- The pure bino, instead, has no couplings and no co-annihilations, such that its cosmological abundance would be too high.

Given that the bino has opposite problems with respect to the higgsino or the wino, it is possible to find a good DM candidate by appropriately mixing them [20]. A mixed bino/wino still has no couplings to the Z , such that it is not interesting for direct detection; furthermore it requires $M_1 \approx M_2$ at the weak scale and is not compatible with unification of gaugino masses, $M_1 \approx M_2 \approx M_3$ at the GUT scale.

We thereby focus on a mixed bino/higgsino. In the limit where we can ignore all other heavier sparticles, its phenomenology is fully described by 3 parameters: the bino mass term M_1 , the higgsino mass term μ (we assume them to be positive) and $\tan \beta$. The observed thermal relic DM abundance is reproduced in the green strip in Fig. 8 (left panel for $\tan \beta = 3$ and right

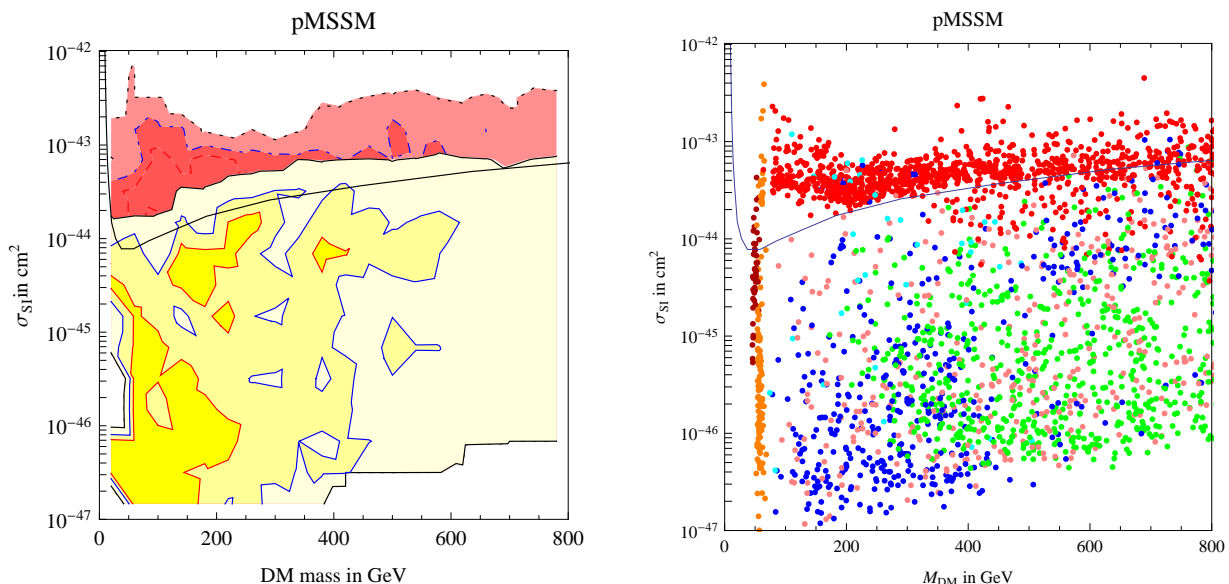


Figure 9: *The pMSSM fit (left panel) in $(M_{\text{DM}}, \sigma_{\text{SI}})$ plane and the corresponding DM generation mechanisms (right panel) in the colour code analogous to Fig. 4 except for three new regions: the pink dots denote “well-tempered” bino/wino; the dark red dots the Z-resonance at $M_{\text{DM}} \approx M_Z/2$; the orange dots denote the light-higgs resonance at $M_{\text{DM}} \approx m_h/2$.*

panel for $\tan \beta = 10$). The region with $M_1 \approx \mu \approx M_Z$ was allowed, but its large direct detection cross section is now disfavored by XENON100 (gray region). An improvement of the XENON100 bound by a factor of few would fully exclude the whole “well-tempered” neutralino scenario, unless the local DM density or the nuclear matrix element f of eq. (12) are significantly lower than what is assumed in our computation.

The minor tilt at $M_{\text{DM}} \approx m_t$ is due to the top quark threshold. At lower masses, the cosmologically allowed region of Fig. 8 is affected by the Z and Higgs resonances ($2M_{\text{DM}} = M_Z$ or m_h respectively, indicated as red curves). At larger masses, the “well-tempered” neutralino region terminates at $\mu \approx 1$ TeV, where the (almost) pure higgsino becomes a good DM candidate.

5.4 Supersymmetry beyond the CMSSM: pMSSM

In order to relax the theoretical constraints of the CMSSM on the SUSY mass spectrum, we also performed a similar analysis for free low energy SUSY parameters of the MSSM. The low energy phenomenological MSSM, pMSSM, is characterized by the three gaugino masses M_1, M_2, M_3 , the higgsino mass μ , the common squark masses $m_{\tilde{q}}$, the left and right-handed slepton masses $m_{\tilde{L}}, m_{\tilde{E}}$, the Higgs mass parameter m_A and by $\tan \beta$. We randomly scan all these parameters.

Fig. 9 shows our results, in the same notations as the corresponding CMSSM figure, Fig. 4. Because the squark and slepton masses are not related any more via the GUT relations, light sleptons become available for a good fit of $(g-2)_\mu$ that dominates the fit. At the same time, heavy squarks can suppress any new contributions to $b \rightarrow s\gamma$. Therefore a wider range of parameters becomes allowed by the global fit, with still a preference for relatively light DM mass, that again mostly corresponds to neutralino/slepton coannihilations (blue dots in Fig. 9b). Again the region disfavored by the new XENON100 data mostly corresponds to the “well-tempered” bino/higgsino (upper red dots in Fig. 9b). Two new regions appear: “well-

tempered” bino/wino (pink dots, at any mass with σ_{SI} below the XENON100 bound), and Z -resonance (dark red dots at $M_{\text{DM}} \gtrsim M_Z/2$). There are now significant overlaps among the various kinds of DM neutralinos and the mechanisms for generating the DM relic abundance are not well separated. Although the pMSSM parameter space is more complicated than the CMSSM one, the results are qualitatively similar.

6 Conclusions

We have performed a fit to the new XENON100 data and, based on that, analyzed several well motivated DM scenarios. We show that XENON100 disfavors the Inelastic Dark Matter interpretation and the light Dark Matter interpretation of the DAMA/LIBRA claim as well as other hints for light DM by CoGeNT and CDMS II.

The first results of the XENON100 experiment exclude part of the parameter space of Dark Matter models coupled to the Higgs boson. The constrained version of the scalar singlet dark matter model (where the DM mass is predicted in terms of DM coupling to the Higgs boson), previously favored by the CDMS hint, gets disfavored. Such model now needs an independent mass term for the scalar singlet around the weak scale, with its associated naturalness problem.

In the context of supersymmetry, we show model independently that the XENON100 data disfavors the generic scenario of “well-tempered” bino/higgsino proposed as a way to get neutralino DM around the weak scale. Within the CMSSM, the XENON100 data excludes small $|\mu|$, small m_A regions of the parameter space previously allowed in the global fit at 3σ level. As a result the “focus-point” region is ruled out and, most likely, the CMSSM charged Higgs boson mass is not accessible at 7 TeV LHC. Furthermore the “Higgs resonance” mechanism for neutralino annihilation, which implies $M_{\text{DM}} \approx m_h/2$ and consequently a relatively light gluino, has now been probed and excluded by LHC data taken during 2011.

The remaining CMSSM best fit parameter space at 3σ level is relatively compact in which the DM relic abundance is generated by the slepton co-annihilation processes. In view of the new LHC bounds, the CMSSM best fit region moves to larger DM mass and consequently to lower direct detection cross section. The remaining CMSSM parameter space is more fine tuned than before.

We obtained qualitatively similar constraints also for the pMSSM, where there is no connection between masses of colored and uncolored sparticles. As a consequence the light Higgs resonance is still allowed.

Note added (27/7/2011). The paper has been fully updated at the light of the new results presented at the EPS-HEP-2011 conference (21–27 July 2011), including data from ATLAS and CMS on supersymmetric particles and about MSSM Higgs bosons, new data from D0, CMS and LHCb about $B_s \rightarrow \mu^+ \mu^-$, and new data from Tevatron on the top quark mass. All those results are available in the web site <http://eps-hep2011.eu>. The new figure Fig. 10 shows the impact of present XENON100 and LHC data on CMSSM global fits. The allowed CMSSM parameter space has moved to considerably large values of the mass parameters m_0 and $M_{1/2}$. As a result, the Higgs resonance region of DM freeze-out is now completely ruled out. The allowed values of $\tan \beta$ are constrained both from below (due to larger sparticle masses, larger $\tan \beta$ is needed to fit the muon $g - 2$ anomaly) and from above (due to the new constraint on $\text{BR}(B_s \rightarrow \mu\mu)$, mainly from LHCb). The DM spin independent direct detection cross section is now predicted to be a factor of few below the present XENON100 bound. As seen in Fig. 7, the overall fit to the CMSSM parameters has become worse and fine tuning of the CMSSM parameters has further increased.

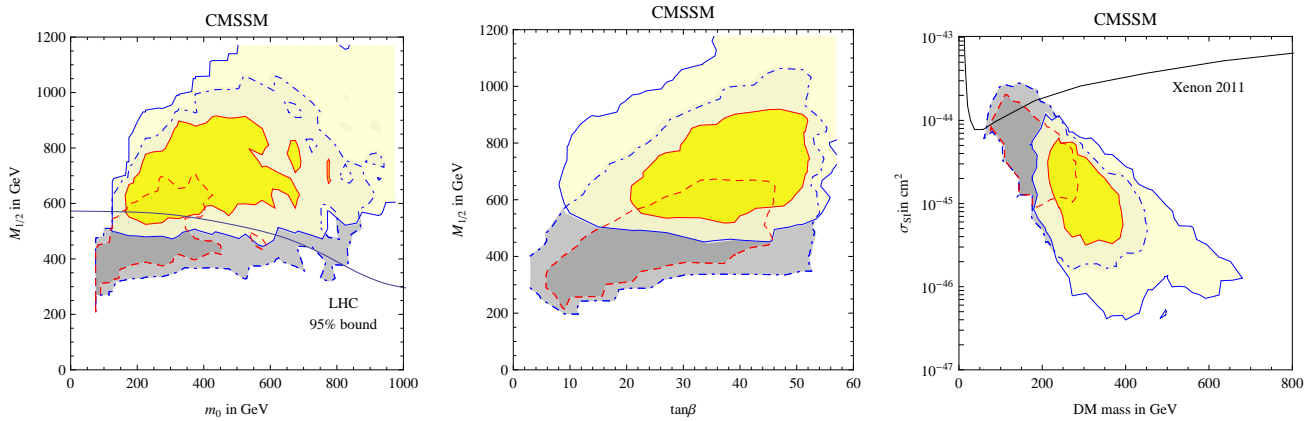


Figure 10: *Impact of the latest XENON100, Tevatron and LHC data with 1.1/fb on CMSSM global fits. In yellow the present global fit at 68 and 95% C.L. for 2 dof; in gray the previous result without such data. Fig. 10a shows that LHC bounds move the best fit region to higher sparticle masses; then a higher $\tan\beta$ is needed to fit the $(g-2)_\mu$ (see Fig. 10b), and a lower direct detection cross section is obtained (see Fig. 10c). The slepton co-annihilation mechanism of DM freeze-out is favored; while now both the “well-tempered” bino/higgsino mechanism as well as the “Higgs resonance” mechanism are no longer allowed by the global fit.*

Note added (18/4/2011). After our fits to the new XENON100 data were performed and studies of iDM completed, a similar dedicated study appeared by the XENON Collaboration itself [58]. Our results agree in that the iDM is strongly disfavoured as an explanation to the DAMA/LIBRA annual modulation signal.

Acknowledgements We thank Alexander Pukhov for valuable communication and for providing us with a new version of Micromegas package. This work was supported by the ESF grants 8090, 8499, MTT8 and by SF0690030s09 project. The work of D.P. is supported by the Swiss National Science Foundation under contract No. 200021-116372. The work of M.F. is supported in part by the European Programme “Unification in the LHC Era”, contract PITN-GA-2009-237920 (UNILHC).

References

- [1] D. Larson *et al.*, *Astrophys. J. Suppl.* 192 (2011) 16 [arXiv:1001.4635].
- [2] G. Jungman, M. Kamionkowski and K. Griest, *Phys. Rept.* 267 (1996) 195 [arXiv:hep-ph/9506380].
- [3] J. R. Ellis, J. S. Hagelin, D. V. Nanopoulos, K. A. Olive and M. Srednicki, *Nucl. Phys. B* 238 (1984) 453.
- [4] G. R. Farrar, P. Fayet, *Phys. Lett. B* 76 (1978) 575-579; S. Dimopoulos, H. Georgi, *Nucl. Phys. B* 193 (1981) 150; L. E. Ibanez, G. G. Ross, *Nucl. Phys. B* 368 (1992) 3-37.
- [5] L. M. Krauss, F. Wilczek, *Phys. Rev. Lett.* 62 (1989) 1221.
- [6] M. Kadastik, K. Kannike and M. Raidal, *Phys. Rev. D* 81 (2010) 015002 [arXiv:0903.2475].
- [7] J. Hisano, K. Ishiwata, N. Nagata and T. Takesako, arXiv:1104.0228.
- [8] M. Cirelli, N. Fornengo, A. Strumia, *Nucl. Phys. B* 753 (2006) 178 [arXiv:hep-ph/0512090].
- [9] CDMS-II Collaboration, *Science* 327 (2010) 1619-1621. [arXiv:0912.3592].
- [10] EDELWEISS collaboration, arXiv:1103.4070.

- [11] XENON100 Collaboration, arXiv:1103.0303.
- [12] DAMA Collaboration, Eur. Phys. J. C 67 (2010) 39 [arXiv:1002.1028].
- [13] CoGeNT collaboration, Phys. Rev. Lett. 106 (2011) 131301. [arXiv:1002.4703].
- [14] D. Tucker-Smith and N. Weiner, Phys. Rev. D 64 (2001) 043502 [arXiv:hep-ph/0101138].
- [15] S. Chang, G. D. Kribs, D. Tucker-Smith, N. Weiner, Phys. Rev. D 79 (2009) 043513 [arXiv:0807.2250].
- [16] E. Aprile *et al.* [XENON100 Collaboration], arXiv:1104.2549 [astro-ph.CO].
- [17] Talk by G. Tonelli (for the CMS collaboration) at the EPS-HEP conference (web site <http://eps-hep2011.eu>), as well as related parallel session talks.
- [18] Talk by D. Charlton (for the ATLAS collaboration) at the EPS-HEP conference (web site <http://eps-hep2011.eu>), as well as related parallel session talks.
- [19] We combine the latest results presented at the EPS-HEP-2011 conference by the D0 ($\text{BR}(B_s \rightarrow \mu^+ \mu^-) = (1.8 \pm 1.0) 10^{-8}$), CMS ($\text{BR}(B_s \rightarrow \mu^+ \mu^-) < 1.9 \cdot 10^{-8}$ at 95% CL with an expected bound of $1.8 \cdot 10^{-8}$) and LHCb ($\text{BR}(B_s \rightarrow \mu^+ \mu^-) < 1.5 \cdot 10^{-8}$ at 95% CL with an expected bound of $1.5 \cdot 10^{-8}$). CMS collaboration, arXiv:1107.5834.
- [20] N. Arkani-Hamed, A. Delgado, G. Giudice, Nucl. Phys. B 741 (2006) 108 [arXiv:hep-ph/0601041]. H. Baer, A. Mustafayev, E.K. Park, X. Tata, JCAP 0701 (2007) 017 [arXiv:hep-ph/0611387]. For previous studies see H. Baer, C. Balazs, A. Belyaev, J. O’Farrill, JCAP 0309 (2003) 007.
- [21] J. L. Feng, K. T. Matchev and T. Moroi, Phys. Rev. Lett. 84 (2000) 2322 [arXiv:hep-ph/9908309]; J. L. Feng, K. T. Matchev and T. Moroi, Phys. Rev. D 61 (2000) 075005 [arXiv:hep-ph/9909334].
- [22] M. C. Smith *et al.*, Mon. Not. Roy. Astron. Soc. 379 (2007) 755 [arXiv:astro-ph/0611671].
- [23] R. H. Helm, Phys. Rev. 104, 1466-1475 (1956).
- [24] G. Plante *et al.*, arXiv:1104.2587 [nucl-ex].
- [25] A. Ianni, G. Pagliaroli, A. Strumia, F. R. Torres, F. L. Villante, F. Vissani, Phys. Rev. D 80 (2009) 043007 [arXiv:0907.1891].
- [26] J. McDonald, Phys. Rev. D 50 (1994) 3637.
- [27] C. Burgess, M. Pospelov, T. ter Veldhuis, arXiv:hep-ph/0011335
- [28] V. Barger, P. Langacker, M. McCaskey, M. Ramsey-Musolf, G. Shaughnessy, Phys. Rev. D 77 (2008) 035005 [arXiv:0706.4311].
- [29] X. He, T. Li, X. Li, J. Tandean, H. Tsai, arXiv:0912.4722.
- [30] M. Farina, D. Pappadopulo, A. Strumia, Phys. Lett. B 688 (2010) 329 [arXiv:0912.5038].
- [31] L.L. Honorez and C.E. Yaguna, JHEP 046 (2010) 1009 [arXiv:1003.3125].
- [32] P. Salucci, F. Nesti, G. Gentile and C. F. Martins, arXiv:1003.3101.
- [33] J. Ellis, K.A. Olive, C. Savage, arXiv:0801.3656.
- [34] J. Giedt, A.W. Thomas, R.D. Young, arXiv:0907.4177.
- [35] D. Toussaint and W. Freeman [MILC Collaboration], Phys. Rev. Lett. 103 (2009) 122002 [arXiv:0905.2432]; R. D. Young and A. W. Thomas, Phys. Rev. D 81 (2010) 014503 [arXiv:0901.3310].
- [36] R. Koch, Z. Phys. C 15 (1982) 161; M. M. Pavan, I. I. Strakovsky, R. L. Workman and R. A. Arndt, PiN Newslett. 16 (2002) 110 [arXiv:hep-ph/0111066].
- [37] G. Belanger, F. Boudjema, A. Pukhov, A. Semenov, Comput. Phys. Commun. 176 (2007) 367-382 [hep-ph/0607059]; G. Belanger, F. Boudjema, A. Pukhov, A. Semenov, Comput. Phys. Commun. 149 (2002) 103-120 [hep-ph/0112278]; G. Blanger, F. Boudjema, P. Brun, A. Pukhov, S. Rosier-Lees, P. Salati, A. Semenov, Comput. Phys. Commun. 182 (2011) 842 [arXiv:1004.1092].
- [38] D. Feldman, K. Freese, P. Nath, B. D. Nelson and G. Peim, arXiv:1102.2548.
- [39] B. C. Allanach, arXiv:1102.3149.

- [40] O. Buchmueller *et al.*, arXiv:1102.4585.
- [41] P. Bechtle *et al.*, arXiv:1102.4693.
- [42] S. Akula, N. Chen, D. Feldman, M. Liu, Z. Liu, P. Nath and G. Peim, arXiv:1103.1197.
- [43] For previous works see, F. Feroz, K. Cranmer, M. Hobson, R. Ruiz de Austri and R. Trotta, arXiv:1101.3296
L. Roszkowski, R. Ruiz de Austri and R. Trotta, Phys. Rev. D82 (2010) 055003. R. Trotta, F. Feroz, M.P. Hobson, L. Roszkowski and R. Ruiz de Austri JHEP 12 (2008) 024.
- [44] J. A. Conley, J. S. Gainer, J. L. Hewett, M. P. Le and T. G. Rizzo, arXiv:1103.1697.
- [45] S. Akula, D. Feldman, Z. Liu, P. Nath and G. Peim, arXiv:1103.5061.
- [46] S. Bethke, Eur. Phys. J. C64 (2009) 689 [arXiv:0908.1135].
- [47] Tevatron Electroweak Working Group, arXiv:1107.5255.
- [48] K. Nakamura *et al.* [Particle Data Group], J. Phys. G 37 (2010) 075021.
- [49] D. Larson *et al.*, Astrophys. J. Suppl. 192 (2011) 16 [arXiv:1001.4635].
- [50] M. Davier, A. Hoecker, B. Malaescu, Z. Zhang, Eur. Phys. J. C71 (2011) 1515. [arXiv:1010.4180].
- [51] M. Misiak *et al.*, Phys.Rev.Lett. 98 (2007) 022002 [arXiv:hep-ph/0609232]. For a recent update see M. Misiak, arXiv:1010.4896.
- [52] O. Buchmueller, R. Cavanaugh, A. De Roeck, J. R. Ellis, H. Flacher, S. Heinemeyer, G. Isidori, K. A. Olive *et al.*, Eur. Phys. J. C64 (2009) 391-415. [arXiv:0907.5568].
- [53] G. Marandella, C. Schappacher, A. Strumia, Nucl. Phys. B715 (2005) 173 [arXiv:hep-ph/0502095].
- [54] A. Strumia, arXiv:1101.2195, updated after the EPS-HEP conference.
- [55] S. Cassel, D. M. Ghilencea, S. Kraml, A. Lessa and G. G. Ross, arXiv:1101.4664.
- [56] O. Buchmueller *et al.*, Eur. Phys. J. C 71 (2011) 1583 [arXiv:1011.6118].
- [57] J. Hisano, S. Matsumoto, O. Saito, M. Senami, Phys. Rev. D73 (2006) 055004 [arXiv:hep-ph/0511118].
M. Cirelli, A. Strumia and M. Tamburini, Nucl. Phys. B787 (2007) 152 [arXiv:0706.4071].
- [58] E. Aprile *et al.*, [XENON100 Collaboration], arXiv:1104.3121.

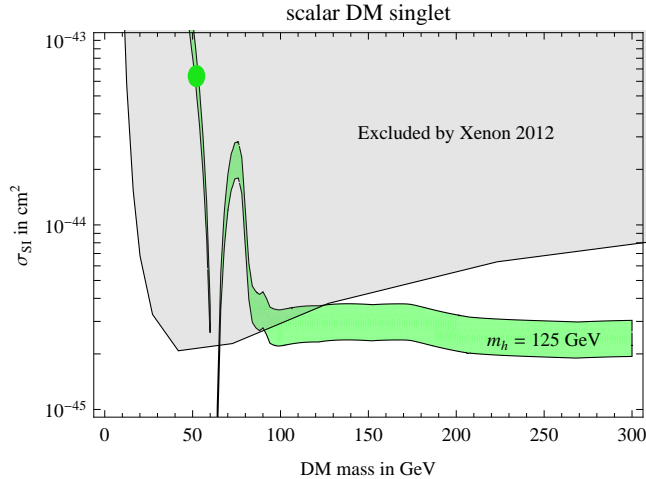


Figure 11: *Update of fig. 3. Predictions of the scalar singlet model.*

Addendum: 2012 data

We update our previous results including the new data released during July 2012 by the XENON100 collaboration [1] (sensitivity to σ_{SI} improved by a factor of 5, see fig. 11) and by the ATLAS and CMS collaborations (stronger bounds on sparticle masses, and the measurement of the Higgs mass: $m_h = 125.5 \pm 0.5$ GeV [2]).

Fig. 11 shows that the scalar singlet DM model considered in section 4 now survives only if DM is heavier than about 100 GeV. In particular this excludes the sub-case where all the DM mass comes from the Higgs vacuum expectation value (green dot in fig. 11).

Coming to supersymmetry, fig. 12 shows that the well-tempered bino/higgsino considered in section 5.3 has been excluded. We recomputed the DM detect detection cross section σ_{SI} now assuming the measured Higgs mass, and we find that the ‘well-tempered’ region along $M_1 \approx |\mu|$ (green strip in the figure, where the DM thermal relic density matches the observed cosmological DM density) is excluded. The allowed region at $|\mu| \approx 1$ TeV corresponds to the pure-Higgsino limit. The allowed region at $M_{\text{DM}} \approx m_h/2$ corresponds to the Higgs resonance region; this possibility is however excluded, in the context of models with gaugino unification, because it implies a too light gluino, excluded by LHC bounds.

Fig. 13 shows in the $(M_{\text{DM}}, \sigma_{\text{SI}})$ plane the CMSSM points that lead to the observed DM abundance and are compatible with present data, including the recent Higgs mass measurement. From a theoretical point of view the CMSSM is a sort of ‘spherical cow’; most of its parameter space has now been excluded, and we are here focusing on its remaining peculiar tails and pieces. In particular, the DM abundance can be explained by alternative fine-tuned mechanisms, here plotted as different colours. In decreasing order of σ_{SI} , red dots correspond to the ‘well-tempered’ bino/higgsino (excluded), extending into the pure-Higgsino limit. Cyan dots correspond to DM annihilations via couplings enhanced by $\tan \beta \approx 50$. Green dots correspond to annihilations via heavy Higgs resonances with large $\tan \beta$. Blue points correspond to slepton co-annihilation and magenta points to stop co-annihilation. No real best-fit region emerges.

References

- [1] XENON100 Collaboration, arXiv:1207.5988.
- [2] ATLAS Collaboration, arXiv:1207.7214. CMS Collaboration, arXiv:1207.7235.

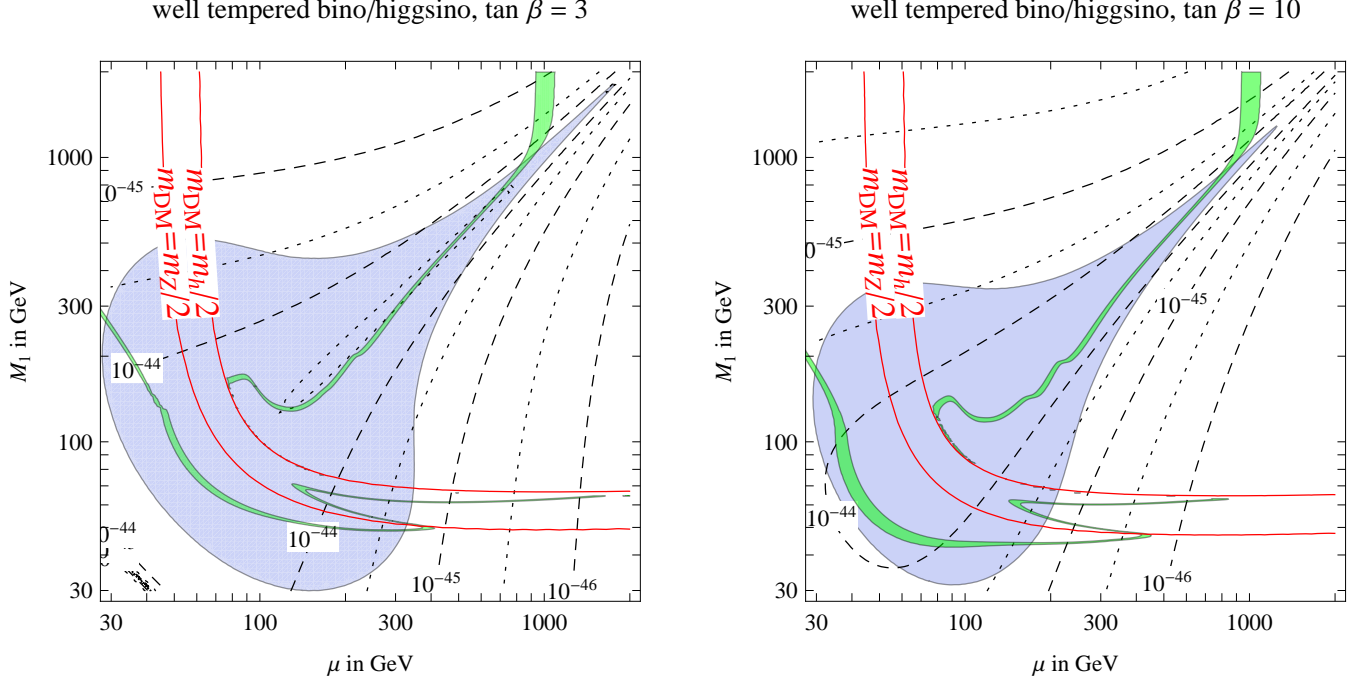


Figure 12: (Update of fig. 8). Model independent “well-tempered” neutralino scenario for $m_h = 125$ GeV. The 3σ range for the cosmological DM abundance is reproduced within the green strip. The gray region is excluded by XENON100 [16].

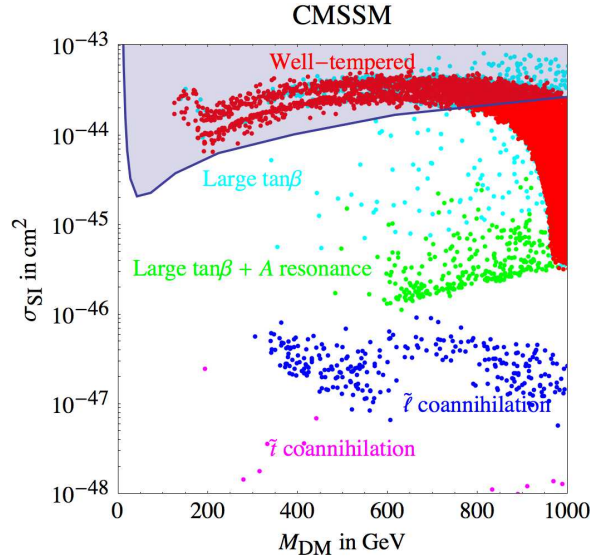


Figure 13: (Update of fig. 5). The $(M_{\text{DM}}, \sigma_{\text{SI}})$ plane in the CMSSM. Points with $\Delta\chi^2 < 5^2$, colored according to the DM annihilation mechanism.